Investigating the effect of observation interval on GPS, GLONASS, Galileo and BeiDou static PPP

Sermet Ogutcu*[1] , Abbas Qader Shakor [1] , Haitham Talib Farhan [1]

[1]Necmettin Erbakan University, Faculty of Engineering, Department of Geomatics Engineering, Konya, Turkey

ABSTRACT

GNSS observation intervals can be tuned from low rate to high rates (such as 300 to 1 s) for the specific applications. In this study, the effect of sampling intervals of 1, 5, 15, and 30 s on the convergence time and positioning accuracy of static precise point positioning is investigated using high-rate data from 26 IGS (International GNSS Service)-MGEX (Multi-GNSS Experiment) stations over a three-week period in 2020. Six different GNSS constellations – namely, GPS-only, GLONASS-only, Galileo-only, BeiDou-2-only, BeiDou-3-only, and multi-GNSS (GPS+GLONASS+Galileo+BeiDou-2+BeiDou-3) – are processed for static PPP. The results show that the use of higher rate of observation intervals significantly reduces the PPP convergence time for each GNSS constellation. Maximum improvements between 30 s and 1 s are found to be 55%, 60%, and 55% for north, east, and up components, respectively, for Galileo PPP. However, the results of positioning accuracy indicates that the use of higher rate of observation intervals slightly degrades the PPP converged positioning accuracy for each GNSS constellation except for BDS-3 and multi-GNSS PPP modes. The results demonstrate that the satellite clock interpolation error is mainly responsible for the degradation in accuracy at the higher rate of observation intervals compared with the orbit interpolation error.

1. INTRODUCTION

Precise point positioning (PPP) (Zumberge et al. 1997) has received significant attention over recent decades. PPP is a powerful tool for many scientific research, such as atmospheric and ionospheric studies (Ge et al. 2021a; Ma and Verhagen, 2020; Wang et al. 2020), monitoring of deformation, tectonic and earthquake activities (Vazquez-Ontiveros et al. 2020; Alcay et al. 2019; Mendoza et al. 2012), geophysical studies (Geng et al. 2017) and, time transfer (Ge et al. 2020). One of the most important aspects of PPP compared with the precise differential positioning is that positioning accuracy of mm to cm can be obtained using a single receiver in the static and kinematic modes, respectively (Yigit et al. 2021; Yigit et al. 2014; Alcay and Turgut 2021). However, the convergence time in PPP still poses a challenging problem. To obtain three-dimensional accuracy at the cm level, an observation session of approximately 30 min is needed (Liu et. 2019). The PPP convergence time can be improved through the use of ambiguity resolution (AR) (Laurichesse and Blot, 2016; Grinter et al. 2020; Atiz et al. 2021), multi-frequency and multi-GNSS observations, (Psychas et al. 2020; Ogutcu, 2020) and, ionospheric and atmospheric constraints (Zhang et. 2013; Aggrey and Bisnath, 2019).

High-rate GNSS positioning (with frequency of 1 Hz or higher) has become possible following the evolution of the GNSS receivers, and has been used effectively in GPS seismology (Xu et al. 2013), structural health monitoring (Yigit et al. 2021), and the detection of dynamic displacements (Paziewski et al. 2018).

Unlike in relative precise positioning, errors in the satellite orbit and clock directly lump to the station coordinates for PPP. Satellite orbit and clock interpolation is a prerequisite if the observation sampling interval is lower than the interval of the orbit and clock products. Since the orbit is a very smooth trajectory, the orbit interpolation error is generally insignificant. Yousif and El-Rabbany (2007) investigate the interpolation error of GPS orbit using IGS precise

orbit spaced at 15 min. It is found that GPS orbit interpolation can be conducted with a sub-mm level interpolation error. Zheng and Zhang (2020) analyze the orbit interpolation error of GPS, GLONASS and BeiDou (BDS-2) real-time broadcast ephemeris. They found that orbit interpolation error is less than 1e-4 m for GPS, GLONASS and BeiDou constellations. Due to the instability of the GNSS clock biases, a smooth trend in GNSS clock biases is not seen. Since unpredictable clock variations can occur even within a short period, high-order polynomial interpolation cannot be applied efficiently for clock biases, unlike for orbit interpolation. The presence of these random noise characteristics means that linear interpolation is generally chosen for the interpolation of the clock biases (Montenbruck et al. 2005).

Geng et al. 2016 investigate the interpolation error in BeiDou (BDS-2) clock bias data using samplings of 5, 30, and 300 s with respect to a clock bias solution of 1 s sampling. The results show that 0.04 ns (12 mm), 0.02 ns (6 mm), and 0.01 ns (3 mm) interpolation errors are found for 300, 30, and 5 s sampling clock bias data, respectively. Guo et al. 2010 investigates the effect of IGS precise clock products with sampling at 5 min, 30 s and 5 s on the static and kinematic PPP using an observation interval of 30 s. Positioning errors at the mm and cm levels for clock products of 5 min and 30 s are obtained for static and kinematic PPP, respectively, due to the interpolation error of the clock biases with respect to a clock product of 5 s. Takasu (2006) interpolate GPS clock biases of 30 s and 5 min to create sampling clock biases of 1 s. These interpolated sampling clock biases are then compared with the raw 1 s clock biases estimated using the high-rate data from GPS stations. It is found that the interpolation error is around 0.1 – 0.3 ns (3 – 9 cm) for a sampling clock product of 5 min and 0.01 – 0.03 ns (3 – 9 mm) for a sampling clock product of 30 s.

A few studies have been conducted on the effects of the observation interval for PPP. Bahadur and Nohutcu 2020 investigate the effect of high-rate sampling observation on the convergence time and positioning accuracy of static PPP using 10 IGS-MGEX stations over a one-week period. GPS, GLONASS and GPS+GLONASS+GALILEO+BeiDou (BDS-2) constellations are processed separately. The results show that the use of high-rate observations significantly reduced the convergence time for the three PPP processing modes. The results indicate that use of high-rate observations contributed to the positioning accuracy within the first 30 min for each PPP processing mode. It is found that after the converged state has been reached, no improvement in accuracy for each PPP processing mode. Erol et al. 2020 conduct quasi-kinematic PPP over 4 h with GPS+GLONASS constellations using sampling intervals of 0.2, 0.5, 1, 5, 10, 30, 60, and 120 s for a single geodetic control point. The results show that the RMSE of the height component was significantly increased at higher sampling rates, while the RMSE of the horizontal component was not changed significantly. A convergence analysis was not conducted in this study. Ge et al. 2018 investigate the relationship between the sampling rate and convergence time using the simulated low Earth orbit (LEO) enhanced GNSS constellations (GPS+BDS-2), using sampling intervals of 30, 10, 5, and 1 s. The results indicate that the convergence time became shorter as the sampling interval increased. 41%, 44% and 46% acceleration in the convergence time were reported for the north, east and up components, respectively. Zuoya et al. 2010 analyses the relationship between the sampling rate and PPP convergence time, using 12 stations in a GPS network from Shanghai, China. Sampling intervals of 1 and 30 s were used. It is found that the convergence time at a sampling interval of 1 s is significantly decreased compared with a sampling interval of 30 s. Glaner and Weber, 2021 investigate the effect of 1 and 30 s sampling rates on the convergence time of PPP with AR using GPS+Galileo. They found that the 1 s sampling rate accelerated the convergence time for two-dimensional by 45 to nearly 60 percent compared with the 30 s sampling rate solutions.

The literature review shows that there still are no in-depth discussions of the effect of a higher sampling rate on the PPP positioning accuracy and convergence time. Moreover, no studies have addressed the effects of higher sampling rates for each GNSS constellation separately (GPS, GLONASS, Galileo, BeiDou-2 and, BeiDou-3). The objective of this study is therefore to investigate the effect of sampling intervals of 1, 5, 15, and 30 s on the PPP convergence time and positioning accuracy, using six different GNSS constellations (i.e., GPS, GLONASS, Galileo, BeiDou-2, BeiDou-3, and multi-GNSS). In the following section, a functional model of PPP is briefly introduced. Details of the data processing steps are given in Section 3. The results are summarized in Section 4, and the conclusions are presented in the final section.

2. FUNCTIONAL MODEL OF IONOSPHERE-FREE PPP

The ionosphere-free (IF) carrier phase and code observations are used in traditional PPP. The IF equations are written for the phase and code data as follows (Leick et al., 2015):

$$P_{IF,r}^{s,j} = \rho + c * \left(dt_r - dt^{s,j}\right) + d_{trop} + HD_{P,r,IF} - HD_{P,IF}^{s,j} + \epsilon_{P,IF}^{s,j} \tag{1}$$

$$\phi_{IF,r}^{s,j} = \rho + c * \left(dt_r - dt^{s,j}\right) + d_{trop} + \lambda_{IF}^{s,j} * N_{r,IF}^{s,j} + HD_{\phi,r,IF} - HD_{\phi,IF}^{s,j} + \epsilon_{\phi,IF}^{s,j} \tag{2}$$

where the superscript s and j denote the satellite and GNSS index (G:GPS, R:GLONASS, E:Galileo and C:BeiDou), the subscript r denotes the receiver, $P_{IF,r}^{s,j}$ and $\phi_{IF,r}^{s,j}$ are the IF combinations of code and carrier phase observations, ρ is the pseudorange in meters, c is the speed of light in meters per second, dt_r is the receiver clock offset in seconds, $dt^{s,j}$ is the satellite clock offset in seconds, d_{trop} is the tropospheric delay in meters, $\lambda_{IF}^{s,j}$ is

the IF wavelength, $N_{IF}^{s,j}$ is the IF carrier phase initial ambiguity, $HD_{P,r,IF}^{s,j}$ and $HD_{\emptyset,IF}^{s,j}$ are the IF code and carrier phase receiver hardware delay in meters, $HD_{P,IF}^{s,j}$ and $HD_{\emptyset,IF}^{s,j}$ are the IF code and carrier phase satellite hardware delay in meters and $\epsilon_{P,IF}^{s,j}$ and $\epsilon_{\emptyset,IF}^{s,j}$ are the IF code and carrier phase measurement noise. Thanks to MGEX products, satellite orbit and clock errors are eliminated. The pseudorange IF code hardware delay ($HD^{P,s,j,IF}$), originated from satellite, is lumped into the satellite clock offset $dt^{s,j}$. Since clock parameters are estimated using the pseudorange measurements, the receiver clock estimate can absorb the receiver pseudorange hardware delay $HD_{P,r,IF}$ of IF combination. Satellite and receiver IF phase delay ($HD^{\emptyset,s,j,IF}$ and $HD_{\emptyset,r,IF}$) are lumped into the float ambiguity parameter (Xiao et al., 2019).

The IF code and phase equations can be written as:

$$P_{IF,r}^{s,j}=(f1^2 * P1^{s,j} - f2^2 * P2^{s,j})/(f1^2 - f2^2) \qquad (3)$$

$$\emptyset_{IF,r}^{s,j}=(f1^2 * \emptyset1^{s,j} - f2^2 * \emptyset2^{s,j})/(f1^2 - f2^2) \qquad (4)$$

where $f1$ and $f2$ are two frequencies of phase data, $P1$, $P2$, $\emptyset1$, and, $\emptyset2$ are the pseudorange and carrier phase data on the two frequencies. IF wavelength (λ_{IF}) and float ambiguity ($\widetilde{N_{IF}}$) can be expressed as:

$$\lambda_{IF} = \frac{c}{f1+f2} \qquad (5)$$

$$\widetilde{N_{IF}}=N1 - \frac{1}{2} * \left(\frac{\lambda_{WL}}{\lambda_{IF}} - 1\right) * (N2 - N1) \qquad (6)$$

where λ_{WL} is the wide-lane wavelength. $N1$ and $N2$ are the float ambiguities of first and second frequencies.

Wavelength of wide-lane can be written as:

$$\lambda_{WL} = \frac{c}{f1-f2} \qquad (7)$$

When multi-GNSS PPP is conducted, the inter-system biases (ISBs) between GPS and other constellations (GLONASS, Galileo, and BDS) need to be estimated. In this study, the ISB is estimated as an unknown parameter for Galileo and BeiDou constellations, while it is estimated for each individual GLONASS satellite epoch by epoch, due to the use of Frequency Division Multiple Access (FDMA) design. A stochastic model of the ISB is chosen as random-walk process with a spectral density of $0.0017 \, m/\sqrt{sec}$. The estimated parameters of the multi-GNSS PPP can be expressed as:

$$X = [\bar{x}, dt_r, Z_{wet}, Grad_{ns}, Grad_{ew}, \widetilde{N_{IF}}, ISB_{G-R}, ISB_{G-E}, ISB_{G-C}] \qquad (8)$$

where Z_{wet}, $Grad_{ns}$, and $Grad_{ew}$ are the zenith wet delay, north-south and east-west tropospheric gradients, respectively.

3. DATA PROCESSING

Twenty-six high-rate IGS MGEX stations were chosen in this study (Fig. 1).
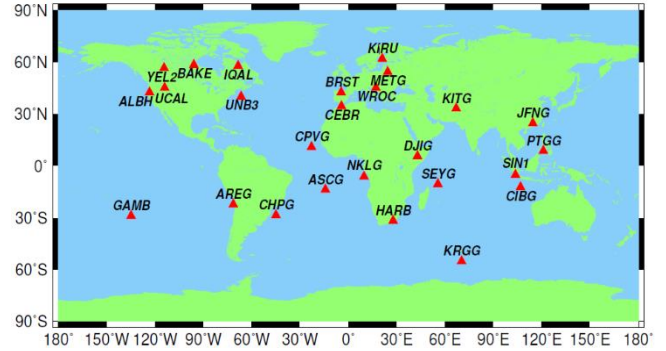
Figure 1. Geographic distribution of the chosen high-rate IGS-MGEX stations

When choosing these stations, a check was made to ensure that all of them could collect GPS-GLONASS-Galileo data, and that all of the stations (eight in total) located in the Asia-Pacific region could collect BDS-2 data. Since Full Operational Capability (FOC) for BDS-3 was achieved on July 31, 2020 (Zhu et al. 2021), a limited number of high-rate IGS-MGEX receivers can track data from all the available BDS-3 satellites. The brand and firmware version of the receiver affect the data tracking performance of BDS-3 constellation (Cao et al. 2020). Therefore, among the twenty-six high-rate IGS MGEX stations, five stations (AREG, KRGG, NKLG, PTGG, and YEL2) which can track much more BDS-3 satellites compared with the other stations were used for BDS-3 and multi-GNSS PPP modes. The mean number of BDS-3 satellites for which data could be collected by these stations was seven for each epoch. These five stations were used for BDS-3-only and multi-GNSS PPP processes. A three-week period (DOY: 95-116) in 2020 was chosen for each PPP process. The frequency and epoch availability of each RINEX file was checked using in-house software, and files with less than 99% epoch and 95% frequency availabilities were discarded from the processing. In this way, the integrity of the high-rate data (1 s) was preserved, and the effects of data loss for the various observation intervals were eliminated. As a result, 12% of all the RINEX data were excluded from PPP processing. The PPP processes were conducted using GipsyX software, developed by the NASA Jet Propulsion Laboratory (JPL) (Bertiger et al. 2020). Six different PPP processing modes i.e., GPS-only (G), GLONASS-only (R), Galileo-only (E), BDS-2-only (C2), BDS-3-only (C3), and multi-GNSS (GREC2C3) were processed for each station and period. GFZ (GeoForschungsZentrum Potsdam)-MGEX orbit and clock products were used for the PPP processes. The temporal resolutions of GFZ-MGEX products are 300 and 30 s for satellite orbit and clock biases, respectively. The convergence time and positioning accuracy were computed for each PPP mode, using sampling intervals of 1, 5, 15, and 30 s. The convergence time was computed by restarting the estimation filtering every hour, meaning that 24 independent batches of observation length 1 h were therefore processed for each day and each station. The

criterion of the convergence time was determined as to when the error of north, east, and up components is less than 0.1 m for the next consecutive 10 epochs. The static positioning accuracy was computed using 12 independent batches with an observation length of 2 h

for each day and each station. The reference coordinates of the IGS-MGEX stations were taken from the IGS weekly solutions. The PPP processing parameters were given in Table 1.

Table 1. PPP processing parameters

Adjustment model	Kalman filter with square root information filter (SRIF) (Bierman, 1977).
Epoch interval	1-s, 5-s, 15-s, and 30-s
Filter	Forward filtering with backward smoothing
Elevation cut-off angle	7°
Orbit and clock interpolation:	Orbit: 11th degree using Neville's interpolation algorithm (Mühlbach, 1978) Clock: 1th degree
Weighting strategy	Initial phase precision: 0.01m for GPS, GLONASS, Galileo, BeiDou-2 MEO, and BeiDou-3 MEO (0.015 m and 0.02 m for IGSO and GEO, respectively). A priori code precision: 1 m for GPS, Galileo, GLONASS, BeiDou-2 MEO, and BeiDou-3 MEO (1.5 m and 2 m for IGSO and GEO, respectively) Elevation dependent weighting: $1/\sqrt{\sin(E)}$
Satellite phase center	Up-to-date IGS14.atx
Receiver phase center	The phase center offset and phase center variation of GPS and GLONASS computed using IGS14.atx. Corrections for the GPS are also used for the Galileo and BeiDou signals.
Ionospheric effect	Removed by IF linear combination (for first-order).
Phase Ambiguities	Estimated as real-value constants for the continuous arc.
Intra-Frequency Bias	Up-to-date daily DCB file was used for GPS C1-P1
Troposphere	GPT2 model
Zenith wet delay estimation	Random walk 0.5 mm/sqrt(sec)
Horizontal delay gradients estimation	Random walk 0.05 mm/sqrt(sec)
Phase windup	Corrected
Solid earth, ocean tide loading and polar tides	IERS conventions, 2010
Relativistic corrections	Periodic clock corrections and gravitational bending (shapiro delay) were applied (Hećimović, 2013)
Cycle-slip	Detected by Melborne-Wubbena combination.
Receiver clock jump	Corrected
Eclipse strategy	Modelled attitude was used for the noon and shadow maneuvers of GNSS satellites

4. RESULTS AND ANALYSIS

In this section, the convergence time and positioning accuracy are evaluated for each PPP mode. For ease of understanding, the mean convergence time for each coordinate component is given for a sampling rate of 30 s for each PPP mode. Then, the improvements in the convergence time with respect to sampling intervals of 1, 5, and 15 s are given. The RMSEs of the positioning accuracy are given for 2 h static PPP, for each PPP mode and sampling interval. If the error in any coordinate component (north, east or up) was greater than 30 cm, this solution was assumed to be an outlier and was discarded from the RMSE computation for static PPP.

4.1 Results for the convergence time

Table 2 summarizes the mean convergence times for each PPP mode, using an observation interval of 30 s and independent batches of observation length 1 h.

As can be seen from Table 2, the convergence time was significantly reduced for the multi-GNSS (GREC2C3) combination compared with the other constellations. It should be emphasized that the number of GNSS stations

used in this study was the same (26) for GPS, GLONASS and Galileo PPP, but different for BDS-2 (eight) and BDS-3/multi-GNSS (five). Therefore, a statistically robust comparison of convergence times between the PPP processing modes (except for GPS, GLONASS and Galileo) cannot be carried out. Since the focus of this study is on the effect of the observation interval, this does not negatively affect this experiment. Figure 2 shows the improvements in north, east and up components of the convergence time using sampling intervals of 15, 5, and 1 s with respect to an observation interval of 30 s for each PPP mode.

Table 2. Mean convergence time for 30 sec observation intervals (unit: minute)

GNSS	Convergence time for 30 sec intervals		
	north	east	up
GPS	10.3	23.2	22.1
GLONASS	16.6	27.1	24.0
Galileo	12.5	25.6	24.9
BDS-2	15.0	29.3	23.2
BDS-3	13.5	20.4	20.7
Multi-GNSS	4.3	9.4	9.4
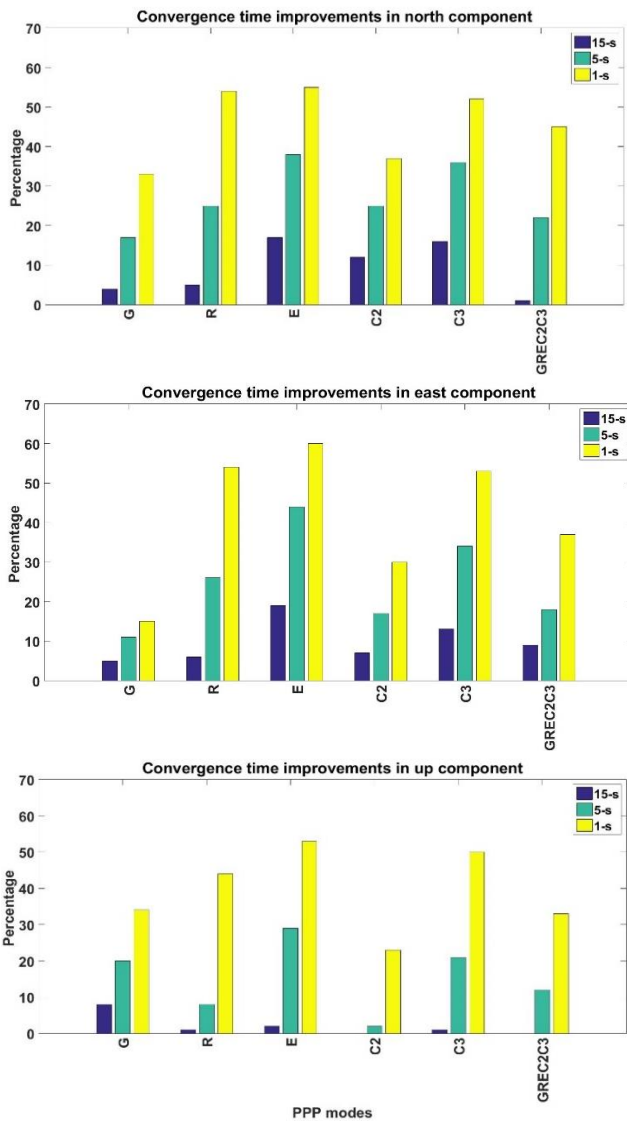
Figure 2. Convergence improvements of 15-s, 5-s, and 1-s sampling rates with respect to 30-s sampling rate

From Figure 2, it can be seen that sampling intervals of 5 and 1 s significantly reduced the convergence time for each coordinate component, for each PPP mode. The effect of a sampling interval of 15 s on the convergence time for the C2, C3, and GREC2C3 PPP modes was significantly lower than for the G, R, and E PPP modes. The biggest reduction in the convergence time using an interval of 1 s was seen for the Galileo constellation in each coordinate component. Approximately 55%, 60%, and 55% improvements in a sampling interval of 1 s were computed for north, east, and up components for the Galileo constellation, respectively. Since the number of MEO satellites in BDS-3 orbit are much higher than BDS-2 orbit, the improvement in the convergence time of BDS-3 with high-rate sampling was much larger than for BDS-2, due to the larger changes in the BDS-3 satellite geometry compared with BDS-2. Since orbital speed is one of the factors that affects the convergence time, the mean orbital speed was computed for each GNSS constellation for the test period, and these values are given in Table 3. The satellite orbital speed in the ECEF frame was computed from the satellite variation between two close epochs (0.0001 s).

Table 3. Orbital speed of each GNSS constellation in ECEF frame

Constellation	Orbital Speed (km/sec)
GPS	2.97
GLONASS	3.37
Galileo	2.75
BDS-2 MEO	2.87
BDS-2 IGSO	2.12
BDS-3 MEO	2.86
BDS-3 IGSO	2.21

As can be seen from Table 3, GLONASS had the highest orbital speed among the other GNSS. Since the orbital speed for Galileo was lower than for GPS and GLONASS, the highest improvement in the convergence time for Galileo cannot be explained solely based on the orbital speed, and therefore needs further investigation. The lowest contribution of the high sampling rate to the convergence time was observed for the C2 and GREC2C3 PPP modes.

4.2 Results for positioning accuracy

Tables 4 shows the RMSEs for each static PPP mode using 12 independent batches with an observation length of 2 h for each day and each station, at sampling intervals of 30, 15, 5, and 1 s.

Table 4. RMSEs of static PPP modes using 2-h observation sessions (Unit: cm)

Sampling rate	GPS		
	north	east	Up
30-s	0.9	2.9	3.3
15-s	0.9	3.0	3.3
5-s	1.0	3.4	3.4
1-s	1.2	3.8	3.8
Sampling rate	GLONASS		
	north	east	Up
30-s	2.3	5.6	6.0
15-s	2.3	5.9	6.0
5-s	2.3	6.4	6.2
1-s	2.7	7.2	6.1
Sampling rate	GALILEO		
	north	east	Up
30-s	1.4	2.9	3.6
15-s	1.4	3.0	3.6
5-s	1.4	3.0	3.6
1-s	1.5	3.3	4.0
Sampling rate	BeiDou-2		
	north	east	Up
30-s	2.2	4.4	5.7
15-s	2.6	4.6	5.8
5-s	2.2	4.5	5.3
1-s	2.0	4.7	5.5
Sampling rate	BeiDou-3		
	north	east	Up
30-s	2.9	5.8	6.3
15-s	2.9	5.8	6.2
5-s	2.8	5.4	6.2
1-s	2.8	5.6	6.3
Sampling rate	Multi-GNSS (GREC2C3)		
	north	east	Up
30-s	1.1	4.3	4.8
15-s	1.1	4.2	4.8
5-s	1.0	3.7	4.8
1-s	1.0	3.8	4.8

The results for the RMSEs show that the effect of the observation sampling interval on the converged positioning accuracy was rather small compared with that of the convergence time. Except for BDS-2 and multi-GNSS, higher sampling rates slightly reduced the positioning accuracy for each PPP mode. This loss of accuracy is much more evident between sampling intervals of 30 and 1 s. Except for this, no significant changes in accuracy were found between the 30 s interval and higher sampling intervals (15 and 5 s). A statistically robust comparison of the accuracies of the PPP processing modes cannot be carried out (except for GPS, GLONASS and Galileo) due to the small numbers of GNSS stations used for BDS-2 (eight) and BDS-3/multi-GNSS (five). To analyze the main sources of the loss of accuracy, the orbit and clock interpolation errors were investigated. Since the orbit (300 s) and clock (30 s) GFZ MGEX products used in this study had the maximum temporal resolution, the orbit product was resampled to 600 s and the clock product to 60 s. Then, the GNSS 600 s satellite positions and 60 s clock biases were interpolated to intervals of 300 s and 30 s, respectively, to investigate the interpolation error for each GNSS system. A Newton-Neville interpolation (Krogh, 1970) with 11th degree and first-order linear interpolation were used for the orbit and clock interpolations, respectively. These interpolations models were the same as those used for PPP processing. Tables 5 and 6 display the mean RMSEs for the interpolation errors in the orbit and clock biases over the test period. The maximum computed interpolation errors are also given along with the RMSEs.

Table 5. RMSEs and maximum interpolation errors of orbit interpolation (Unit: mm)

GNSS System	RMSE_ΔX	RMSE_ΔY	RMSE_ΔZ
GPS	0.76	0.68	0.66
GLONASS	0.74	0.74	0.66
GALILEO	0.66	0.71	0.69
BDS-2-MEO	0.76	0.81	0.51
BDS-3-MEO	0.75	0.65	0.72
BDS-2-IGSO	0.78	0.60	0.69
BDS-3-IGSO	0.65	0.60	0.75
BDS-2-GEO	0.70	0.70	0.58
GNSS System	Max_ΔX	Max_ΔY	Max_ΔZ
GPS	23.0	11.1	10.0
GLONASS	9.8	11.4	8.2
GALILEO	9.8	10.7	10.0
BDS-2-MEO	8.0	12.4	5.3
BDS-3-MEO	13.5	10.7	11.9
BDS-2-IGSO	9.0	8.3	13.4
BDS-3-IGSO	7.9	6.1	9.3
BDS-2-GEO	8.7	8.7	4.7

In Table 5, RMSE_ΔX, RMSE_ΔY and RMSE_ΔZ represent the computed mean RMSEs of the orbit interpolation errors for all satellites within each GNSS system, in X, Y and Z ECEF components, respectively, over the test period. Max_ΔX, Max_ΔY and Max_ΔZ represent the computed maximum orbit interpolation errors in X, Y and Z ECEF components, respectively, for the test period. As can be seen from Table 5, the RMSEs of orbit interpolation errors are in the sub-mm range for each

GNSS system. The maximum orbit interpolation errors are at the level of a few cm in all three dimensions for each GNSS system.

Table 6. RMSEs and maximum interpolation errors of clock interpolation (Unit: mm)

GNSS System	RMSE_Δdt^s	Max_Δdt^s
GPS	13.6	150.0
GLONASS	14.1	115.0
Galileo	2.30	34.9
BeiDou-2-MEO	4.05	19.7
BeiDou-3-MEO	1.77	22.0
BeiDou-2-IGSO	6.18	29.2
BeiDou-3-IGSO	2.31	12.1
BeiDou-2-GEO	3.91	24.6

In Tables 6, RMSE_Δdt^s and Max_Δdt^s represent the computed mean RMSEs for the clock interpolation errors and the maximum clock interpolation errors for all satellites, respectively, for each GNSS system over the test period. Clock interpolation errors (seconds) are scaled to speed of light to convert to mm. As expected, the clock interpolation errors are significantly higher than the orbit interpolation errors for each GNSS. Table 6 shows that the largest clock interpolation errors were observed for GLONASS satellites, and this explains the highest loss of accuracy between sampling intervals of 30 and 1 s for GLONASS PPP. The second largest clock interpolation errors were observed for GPS, and this finding explains the second highest loss of accuracy between intervals of 30 s to 1 s for GPS. Since the clock interpolation errors for Galileo and BDS-2 were significantly smaller than for GPS and GLONASS, the loss of accuracy for Galileo and BDS-2 between intervals of 30 s to 1 s was significantly smaller than for GPS and GLONASS. GNSS clock offset model precision directly affects the clock interpolation errors. The results of the GNSS clock interpolation accuracy in this study supports the overall findings in the study of Cao et al. 2021, Ge et al. 2021b and Ye et al. 2021 related to the GNSS clock offset model precision. It can be observed that this accuracy loss mainly accumulated in the east component. The small improvement in accuracy at a sampling interval of 1 s compared to 30 s was seen for BDS-3 and multi-GNSS PPP modes. The results for the clock interpolation also indicate that the clock interpolation errors for BDS-3 were several times lower than for BDS-2. Since the BDS-2 constellation consists of GEO satellites, changes in the BDS-2 satellite geometry over a short period were significantly smaller than for the other constellations. A slight improvement in accuracy at a sampling rate of 1 s compared to a sampling rate of 30 s was observed for BDS-3 and multi-GNSS PPP modes. Since the accuracy of the initial ambiguity parameters is mainly affecting the length of the convergence time, clock interpolation errors from high-rate sampling intervals are too small to affect the un-converged positioning accuracy.

5. CONCLUSION

This study investigated the effects of high rates of sampling interval on the static PPP convergence time and positioning accuracy. For this purpose, GPS-only,

GLONASS-only, Galileo-only, BeiDou-2-only, BeiDou-3-only, and multi-GNSS (GPS/GLONASS/Galileo/BeiDou-2/BeiDou-3) static PPP were processed using sampling intervals of 1, 5, 15, and 30 s over a three-week period from 26 IGS-MGEX stations. The convergence time was computed using 24 independent batches of observation length 1 h, for each day and each station. The positioning accuracy was computed using 12 independent batches of static observations of length 2 h, for each day and each station.

The results for the convergence time indicate that sampling intervals of 5 s and 1 s significantly reduced the convergence time for each PPP mode compared with a sampling interval of 30 s. The improvement in the convergence time for a sampling interval of 15 s was significantly smaller than for sampling intervals of 5 s and 1s. The improvement in convergence time for a sampling interval of 15 s was below 1% for BDS-2 and multi-GNSS PPP modes. Maximum and minimum improvements in the convergence time using sampling interval of 1 s were observed for the GLONASS/Galileo/BDS-3 and BDS-2 constellations, respectively.

The results for the positioning accuracy showed that there was no significant contribution from sampling intervals of 15, 5 and 1 s to the positioning accuracy at a sampling interval of 30 s. Except for BDS-3 and multi-GNSS PPP modes, a degradation in the accuracy of the converged solutions was evident for the high-rate sampling data, and especially for a sampling interval of 1 s. The results indicated that clock interpolation errors were the main cause of accuracy loss for the higher-rate sampling processes. The largest accuracy loss between sampling intervals of 30 s to 1 s was observed for the GPS and GLONASS satellites, which also had the largest clock interpolation errors among the other GNSS.

This study concludes that most of the time, GNSS observations with high rates of sampling intervals are not necessary to improve the accuracy of the converged solutions. Moreover, it is recommended that the sampling interval should not be lower than the temporal resolution of the clock product used for PPP, in order to avoid a loss of accuracy in the converged solutions. For the applications where the short convergence time or dm-level accuracy is required, the use of high-rate sampling intervals can be an effective way.

ACKNOWLEDMENT

Author contributions

Sermet Ogutcu: Conceptualization, Methodology, Writing-Original draft. **Abbas Qader Shakor:** Convergence analysis. **Haitham Talib Farhan:** Software for orbit and clock interpolation.

Conflicts of interest

The authors declare no conflicts of interest.

REFERENCES

Aggrey J & Bisnath S (2019). Improving GNSS PPP convergence: The case of atmospheric-constrained, multi-GNSS PPP-AR. Sensors, 19(3), 587.

Alcay S & Turgut M (2021). Evaluation of the positioning performance of multi-GNSS RT-PPP method, Arabian Journal of Geosciences, 14, 3, 155, https://doi.org/10.1007/s12517-021-06534-4

Alcay S, Ogutcu S, Kalayci I & Yigit C O (2019). Displacement monitoring performance of relative positioning and Precise Point Positioning (PPP) methods using simulation apparatus. Advances in Space Research, 63(5), 1697-1707.

Atiz O, Ogutcu S, Alcay S, Li P, Bugdayci I (2021). Performance investigation of LAMBDA and bootstrapping methods for PPP narrow-lane ambiguity resolution, Geo-spatial Information Science, https://doi.org/10.1080/10095020.2021.1942236.

Bahadur B & Nohutcu M (2020). Impact of observation sampling rate on Multi-GNSS static PPP performance. Survey Review, 1-10.

Bertiger W, Bar-Sever Y, Dorsey A, Haines B, Harvey N, Hemberger D, … & Willis P (2020). GipsyX/RTGx, a new tool set for space geodetic operations and research. Advances in Space Research, 66(3), 469-489.

Bierman G J (1977) Factorization methods for discrete sequential estimation. Academic, New York.

Cao Y, Huang G, Xie W, Xie S & Wang H (2021). Assessment and comparison of satellite clock offset between BeiDou-3 and other GNSSs. Acta Geodaetica et Geophysica, 1-17.

Cao X, Shen F, Zhang S & Li J (2020). Satellite availability and positioning performance of uncombined precise point positioning using BeiDou-2 and BeiDou-3 multi-frequency signals. Advances in Space Research.

Hećimović Ž (2013). Relativistic effects on satellite navigation. Technical Gazette, 20(1), 195-203.

Erol S, Alkan R M, Ozulu İ M & Ilçi V (2020). Impact of different sampling rates on precise point positioning performance using online processing service. Geo-spatial Information Science, 1-11.

Glaner M & Weber R (2021) PPP with integer ambiguity resolution for GPS and Galileo using satellite products from different analysis centers. GPS Solut 25, 102 https://doi.org/10.1007/s10291-021-01140-z.

Ge Y, Chen S, Wu T, Fan C, Qin W, Zhou F & Yang X (2021a). An analysis of BDS-3 real-time PPP: Time transfer, positioning, and tropospheric delay retrieval. Measurement, 172, 108871.

Ge H, Li B, Wu T & Jiang S (2021b). Prediction models of GNSS satellite clock errors: evaluation and application in PPP. Advances in Space Research.

Ge H, Li B, Ge M, Zang N, Nie L, Shen Y & Schuh H (2018). Initial assessment of precise point positioning with LEO enhanced global navigation satellite systems (LeGNSS). Remote Sensing, 10(7), 984.

Ge Y, Ding S, Qin W, Zhou F, Yang X & Wang S (2020). Performance of ionospheric-free PPP time transfer models with BDS-3 quad-frequency observations. Measurement, 160, 107836.

Geng T, Su X, Fang R, Xie X, Zhao Q & Liu J (2016). BDS precise point positioning for seismic displacements monitoring: benefit from the high-rate satellite clock corrections. Sensors, 16(12), 2192.

Geng J, Jiang P & Liu J (2017). Integrating GPS with GLONASS for high-rate seismogeodesy. Geophysical research letters, 44(7), 3139-3146.

Grinter T, Roberts C & Janssen V (2020). Ambiguity-resolved real-time precise point positioning as a potential fill-in service for sparse CORS networks. Journal of Surveying Engineering, 146(2), 04020007.

Guo F, Zhang X, Li X & Cai S (2010). Impact of sampling rate of IGS satellite clock on precise point positioning. Geo-spatial Information Science, 13(2), 150-156.

Krogh F T (1970). Efficient algorithms for polynomial interpolation and numerical differentiation. Mathematics of Computation, 24(109), 185-190.

Leick A, Rapoport L & Tatarnikov D (2015). GPS satellite surveying. 4th ed. Hoboken: Wiley.

Laurichesse D & Blot A (2016). Fast PPP convergence using multi-constellation and triple-frequency ambiguity resolution. In Proceedings of the 29th International Technical Meeting of The Satellite Division of the Institute of Navigation (ION GNSS+ 2016) (pp. 2082-2088).

Liu X, Jiang W, Li Z, Chen H & Zhao W (2019). Comparison of convergence time and positioning accuracy among BDS, GPS and BDS/GPS precise point positioning with ambiguity resolution. Advances in Space Research, 63(11), 3489-3504.

Ma H & Verhagen S (2020). Precise point positioning on the reliable detection of tropospheric model errors. Sensors, 20(6), 1634.

Mendoza L, Kehm A, Koppert A, Dávila J M, Gárate J & Becker M (2012). The Lorca Earthquake observed by GPS: a test case for GPS seismology. Física de la Tierra, 24(2012), 129-150.

Montenbruck O, Gill E & Kroes R (2005). Rapid orbit determination of LEO satellites using IGS clock and ephemeris products. GPS Solutions, 9(3), 226-235.

Mühlbach G (1978). The general Neville-Aitken-algorithm and some applications. Numerische Mathematik, 31(1), 97-110.

Ogutcu S (2020). Assessing the contribution of Galileo to GPS+ GLONASS PPP: Towards full operational capability. Measurement, 151, 107143.

Paziewski J, Sieradzki R & Baryla R (2018). Multi-GNSS high-rate RTK, PPP and novel direct phase observation processing method: application to precise dynamic displacement detection. Measurement Science and technology, 29(3), 035002.

Psychas D, Verhagen S & Teunissen P J (2020). Precision analysis of partial ambiguity resolution-enabled PPP using multi-GNSS and multi-frequency signals. Advances in Space Research, 66(9), 2075-2093.

Takasu T (2006). High-rate precise point positioning: observation of crustal deformation by using 1-Hz GPS data. In GPS/GNSS Symposium 2006.

Xiao G, Li P, Sui L, Heck B & Schuh H (2019). Estimating and assessing Galileo satellite fractional cycle bias for PPP ambiguity resolution. GPS Solutions, 23(1), 1-13.

Vazquez-Ontiveros J R, Vazquez-Becerra G E, Quintana J A, Carrion F J, Guzman-Acevedo G M & Gaxiola-Camacho J R (2020). Implementation of PPP-GNSS measurement technology in the probabilistic SHM of bridge structures. Measurement, 108677.

Ye Z, Li H & Wang S (2021). Characteristic analysis of the GNSS satellite clock. Advances in Space Research.

Yigit C O, El-Mowafy A, Anil Dindar A, Bezcioglu M & Tiryakioglu I (2021). Investigating Performance of High-Rate GNSS-PPP and PPP-AR for Structural Health Monitoring: Dynamic Tests on Shake Table. Journal of Surveying Engineering, 147(1), 05020011.

Yigit C O, Gikas V, Alcay S & Ceylan A (2014) Performance evaluation of short to long term GPS, GLONASS and GPS/GLONASS post-processed PPP, Survey Review, 46(3), 155-166,

Yousif H & El-Rabbany A (2007). Assessment of several interpolation methods for precise GPS orbit. The journal of navigation, 60(3), 443.

Wang J, Huang G, Zhou P, Yang Y, Zhang Q & Gao Y (2020). Advantages of Uncombined Precise Point Positioning with Fixed Ambiguity Resolution for Slant Total Electron Content (STEC) and Differential Code Bias (DCB) Estimation. Remote Sensing, 12(2), 304.

Xu P, Shi C, Fang R, Liu J, Niu X, Zhang Q & Yanagidani T (2013). High-rate precise point positioning (PPP) to measure seismic wave motions: an experimental comparison of GPS PPP with inertial measurement units. Journal of Geodesy, 87(4), 361-372.

Zhang H, Gao Z, Ge M, Niu X, Huang L, Tu R & Li X (2013). On the convergence of ionospheric constrained precise point positioning (IC-PPP) based on undifferential uncombined raw GNSS observations. Sensors, 13(11), 15708-15725.

Zheng Y & Zhang J (2020). Satellite Orbit Interpolation Algorithm Analysis for GNSS Terminals. In China Satellite Navigation Conference (pp. 310-321). Springer, Singapore.

Zhu Y, Zheng K, Cui X, Zhang Q, Jia X, Zhang M & Fan S (2021). Preliminary analysis of the quality and positioning performance of BDS-3 global interoperable signal B1C/B2a. Advances in Space Research.

Zuoya Z, Xiushan L, Fanlin Y & Xiaoqiang Z (2010). Effect Analysis of GPS Observation and Satellites Clock Bias Sample Rates on Convergence Behavior in PPP. In 2010 International Conference on Multimedia Technology.

Zumberge J F, Heflin M B, Jefferson D C, Watkins M M, & Webb F H (1997). Precise point positioning for the efficient and robust analysis of GPS data from large networks. Journal of geophysical research: solid earth, 102(B3), 5005-5017.